NTNU

Norwegian University of
Science and Technology

Screening of a New Class of Fluorescent Probes for Diagnosis of Amyloid Deposits

Audun Konsmo

Master of Science in Physics and Mathematics
Submission date: June 2018
Supervisor: Mikael Lindgren, IFY

Norwegian University of Science and Technology
Department of Physics

Abstract

The purpose of this project has been to determine photo-physical properties of new and untested fluorescent probes. The probes have a 2,1,3-benzothiadiazole (BTD) ring structure [1] and are derivatives of the previously explored probe BTDSB [2]. The probes are labelled BTD-1, BTD-2, BTD-3, BTD-4, BTD-5, BTD-6, BTD-11, BTD-12, BTD-13 and BTD-14. The probes have been designed for the detection and analysis of amyloid fibrils, which are aggregates of proteins connected to a diverse range of diseases (e.g. Alzheimer's disease, Parkinson's disease and type II diabetes).

Specifically, the lifetimes, absorption spectra, emission spectra and quantum yields of the new probes were measured with toluene as solvent. The new probes had stokes shift of ca. 100 nm or longer and their quantum yields were high (0.59-0.90), with the exception of BTD-5 (0.29). The two-photon absorptions (TPA) were also investigated and interestingly, many of the new probes showed high two-photon absorption cross sections; often more than two times that of the commonly used reference fluorescein [3]. BTD-4 and BTD-5 were especially high, and only BTD-1, BTD-6 and BTD-12 had lower cross sections than fluorescein. In addition, the probes were tested for their affinity for binding to amyloids by measuring their difference in emission with native and fibrillar insulin. BTD-1, BTD-5 and BTD-14 showed a decent increase in emission ($\sim$1.8), while BTD-2 and BTD-3 had a smaller increase ($\sim$1.4) but had a shift of around 35 nm between the fibril and the native peak. BTD-11 had both a decent increase in emission (1.86) and a shift of 24 nm. However, the established probes, DF-9 and ThT, showed a much higher increase in emission: 14.97 and 29.27 respectively. The new probes may still be useful for investigating insulin amyloids because of their high two-photon absorption cross sections. Especially BTD-11 and BTD-14 look promising.

Possible objectives for the future are to investigate the probes with different types of amyloids and, since the new probes all have lifetimes in the nanosecond range, they may be used for fluorescence lifetime imaging (FLIM).

Sammendrag

Formålet med dette prosjektet har vært å undersøke de optiske egenskapene til en serie nye fluorescerende prober. De har en 2,1,3-benzothiadiazole (BTD) ring struktur [1] og er videreutviklet fra proben BTDSB, som har blitt undersøkt tidligere [2]. Probene har fått navnene BTD-1, BTD-2, BTD-3, BTD-4, BTD-5, BTD-6, BTD-11, BTD-12, BTD-13 og BTD-14. Formålet med disse probene er å oppdage og studere amyloid fibriller, som er aggregater av proteiner. Disse er koblet til mange forskjelle sykdommer, som for eksempel Alzheimer, Parkinson og type II diabetes.

Spesifikt, så ble levetider og absorpsjons og emisjons spektrene til probene i toluen målt, og deretter ble kvanteutbytte utregnet. De nye probene har høye verdier (0,59-0,90), med unntak av BTD-5 $(0,29)$, og deres stokes skift var rundt 100 nm eller lengre. To-foton absorpsjon ble også undersøkt, igjen i toluen. Mange av de nye probene hadde gode egenskaper for dette, hvor de ofte hadde mer enn dobbelt så stort tverrsnitt i forhold til fluorescein, som brukes ofte [3]. Spesielt BTD-4 and BTD-5 hadde høye verdier, og bare BTD-1, BTD-6 og BTD-12 hadde lavere tverrsnitt enn fluorescein. I tillegg så ble emisjonen til probene testet sammen med vanlig insulin og insulin-fibriller. BTD-1, BTD-5 og BTD-14 viste en god økning i emittert lys ($\sim$1,8), mens BTD-2 og BTD-3 hadde en mindre økning ($\sim$1,4) men samtidig så flyttet toppen på det emitterte lyset seg med $\sim$35 nm mellom prøven med vanlig insulin og prøven med insulin-fibriller. BTD-11 har både en god økning i signal $(1,86)$ i tillegg til at toppen flytter seg 24 nm. Likevel gir de etablerte probene DF-9 og ThT et mye bedre signal, i og med at de viser en økning på henholdsvis 14,97 and 29,27. De nye probene kan fremdeles være brukbare for å studere insulin amyloider fordi noen av dem har bedre egenskaper for to-foton absorpsjon. Spesielt BTD-11 og BTD-14 er lovende.

Mulige mål for fremtiden er å undersøke hvordan probene binder seg til andre typer amyloider og teste prober med FLIM, siden de nye probene viser levetider på flere nanosekuder.

Preface

This dissertation has been subitted for a Master's degree in Applied Physics at the Norwegian University of Science and Technology. It marks the conclusion of a 10 semester integrated programme in Applied Physics and Mathematics, and amounts to 30 ects-credits in the final semester of the programme. The thesis builds upon results from a 15 ects-credit specialization project from the previous semester, which contributed to a published paper [2]. The work presented in this thesis may contribute to another paper. The project was carried out under the supervision of professor Mikael Lindgren and in collaboration with professor Hammarström's group at Linköping University in Sweden, from which the samples were provided. There they were synthesised by Jun Zhang, a PhD student in chemistry. I spent one week in the lab of professor Hammarström during the semester.

First and foremost, I am grateful to my supervisor for excellent guidance and support. I also wish to thank professor emeritus Thor Bernt Melø for his continuous presence and guidance at the lab and PhD candidate Per Magnus Walmsness for his help, as a lot of laboratory work was done in connection with this dissertation. I would also like to thank professor Hammarström and PhD candidate Jun Zhang for allowing me to spend an educational week at Linköping University.

Audun Konsmo
Trondheim, Norway
June 2018

Contents

List of Figures

List of Tables

Chapter 1

Introduction

A wide array of diseases are associated with the conversion of specific proteins into highly organized fibrillar aggregates called amyloid fibrils. The diseases can be broadly divided into three groups based on where the aggregation takes place: in the brain, where Alzheimer's and Parkinson disease are examples of this, or in a single type of tissue excluding the brain, where Familial Mediterranean fever is an example, or in multiple tissues, where type II diabetes and cataract are two examples of this. These examples all have widely different symptoms and thus the different amyloid fibrils can generate extremely diverse biological functions [8].

Even though the amyloid deposits are known hallmarks of numerous diseases, their actual functional role in disease progression is still unknown. They could be disease-causing, the consequence of cellular disease pathology or even the result of a protective cellular response [9]. One of the reason for this lack of knowledge is that they are difficult to detect, locate and study among the numerous cellular structures, but this becomes easier by the use of techniques such as fluorescence microscopy. This is a powerful method that enables researchers to detect specific proteins and molecules by coupling them to a fluorescent probe [10] and thus making them fluorescent and visible.

The probes are usually hydrophobic and relatively small ligands [11] such as Congo Red, which is a fluorescent dye that has been used for decades to identify amyloids in post-mortem tissue [12]. The molecule X-34 is a derivative of Congo Red, and turned out to be lipophilic and highly fluorescent [13] and therefore an useful fluorescent dye. X-34 is thus a advantageous starting point for development of new and better fluorescent dyes. Four new derivatives were made and their properties related to detection of amyloids were determined [2]. This was in part executed as my specialization project in the 9th semester. One of these new derivatives is called BTDSB and displayed interesting properties. BTDSB is a compund bearing a 2,1,3-benzothiadiazole (BTD) ring, which usually result in a number of desirable characteristics [1]. BTDSB was therefore chosen as a good foundation for continuation.

In this project the properties of BTDSB and it's new derivatives are determined to see if they are usable for the detection and study of amyloid diseases. The new probes are labelled

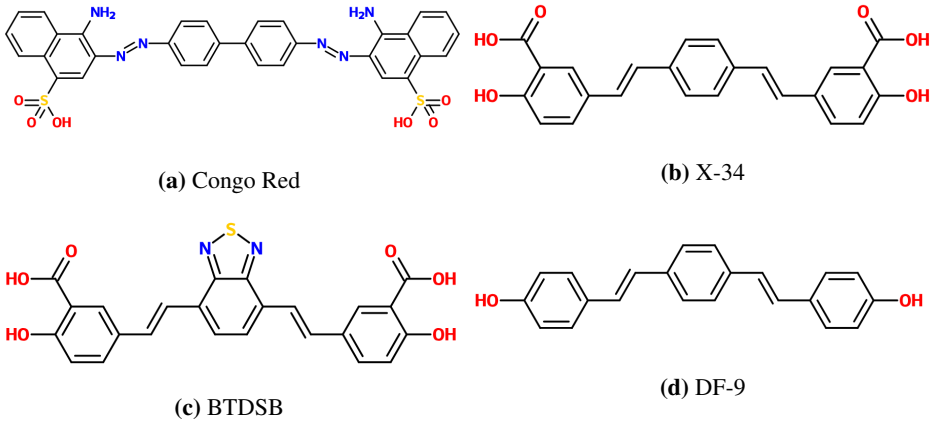

Figure 1.1: The structures of the known samples. They were drawn by the program eMolecules [4].

BTD-1, BTD-2, BTD-3, BTD-4, BTD-5, BTD-6, BTD-7, BTD-11, BTD-12, BTD-13 and BTD-14 and are shown in figure 1.2. They were obtained through a collaboration with Prof. Hammarström's group at Linköping University in Sweden and were synthesised by Jun Zhang, a PhD student in chemistry. I spent one week in the lab of Prof. Hammarström to learn the basics of amyloid production in vitro (of insulin fibrils) and basic characterisation of fibrils in model systems. It is important to test probes such as this [14, 15], because this allows the binding of the probes to be investigated in a controlled environment.

Specifically, the main objective is to investigate these probes to determine their applicability as as diagnostic probes for amyloid aggregates. Their absorption and emission properties in terms of the quantum efficiency will be investigated in addition to determining the characteristics of their life-time and two-photon cross section, which enables use in laser based confocal microscopy. Some examples of the latter are also given with the most promising probes for interaction with insulin amyloids.

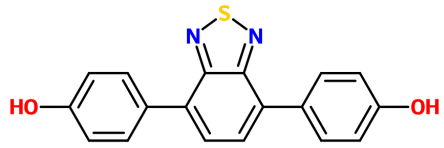

(a) BTD-1

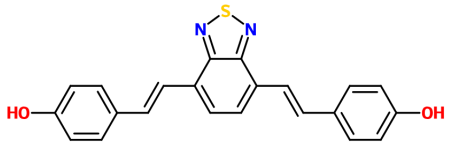

(b) BTD-2

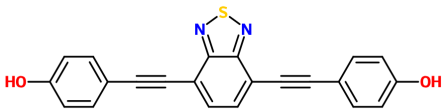

(c) BTD-3

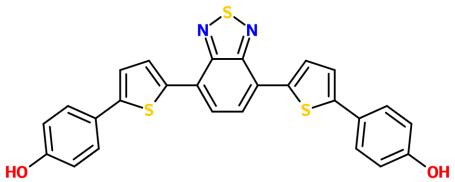

(d) BTD-4

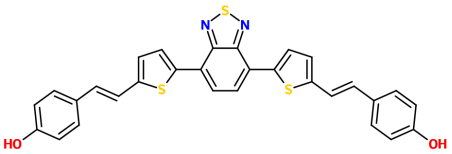

(e) BTD-5

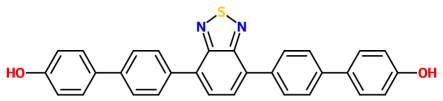

(f) BTD-6

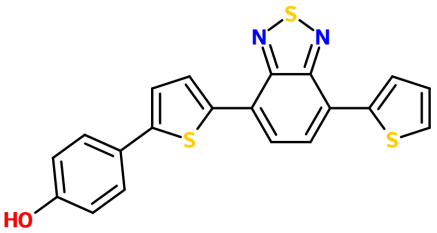

(g) BTD-11

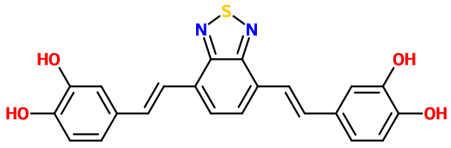

(h) BTD-12

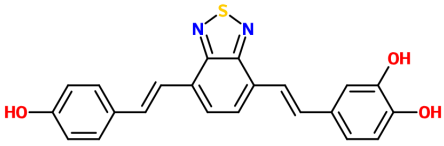

(i) BTD-13

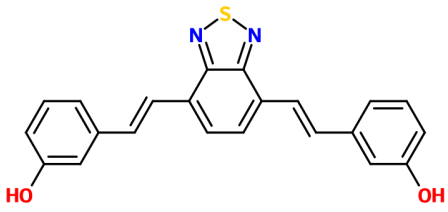

(j) BTD-14

Figure 1.2: The structures of the new probes, where the BTD part can be seen in the centre of the structures. Drawn using the program eMolecules [4].

Chapter 2

Theory of Optical Spectroscopy

2.1 Energy states and absorption of light

A molecule has electrons in orbits around its nuclei. Depending on the positions the electrons, the molecule is in different electronic states with different energies. There is room for two electrons in each orbital where the electrons must have different spins [16]. For all practical purposes, at room temperature the electrons occupy the combination of orbits which results in the lowest energy state for the molecule, called the ground state.

A molecule requires energy to jump from a low energy state to a higher one. This energy may arrive in the form of a photon, where the energy of the photon, $\hbar\omega$ must correspond to the difference between the new and the old energy state of the electron $E_f - E_i$. As the possible energy levels of a molecule or atom is discrete, not all photons will be absorbed. This is expressed in the Fermi golden rule [3]

$$\omega_{i\to f} = \frac{2\pi}{\hbar}|H'_{fi}|^2\delta(E_i - E_f - \hbar\omega), \tag{2.1}$$

where $\omega_{i\to f}$ is the probability per unit time of a transition from a initial lower energy state E_i to a higher final energy state E_f. This probability is zero if the energy of the photon $\hbar\omega$ does not correspond to a possible difference in energy states $E_f - E_i$. H'_{fi} is the quantum mechanical matrix element denoting the strength of the interaction and will be dependent on the properties of the molecule.

The absorption, A, of a molecule is defined by the Beer-Lambert law [3] as

$$A(\omega) = \log(\frac{I_0(\omega)}{I(\omega)}) = \varepsilon(\omega)c\ell, \tag{2.2}$$

where I_0 and I are the intensity of the light before and after the sample. ε is the extinction coefficient, c is the concentration and ℓ is the distance the light travels in through the absorbing medium. The extinction coefficient is a property of the specific molecule and is usually given in $OD \cdot M^{-1} \cdot cm^{-1}$.

We can take a closer look at the transitions by looking at figure 2.1. First of all, an electronic state will have several vibrational sublevels and a vibrational sublevel will again have several rotational sublevels. This is shown in part a of the figure, while part b shows the ground state and the first excited state. The Franck-Condon principle states that because the mass of protons and neutrons is much higher than electrons, it is possible to approximate the electronic transitions as happening without changes in the position of the nuclei [5]. The transition essentially becomes instantaneous and will be a straight vertical line in the figure. The end of the line will be determined by the semiclassical vibrations of a simple harmonic oscillator where the momentum is zero [5], so the turning points.

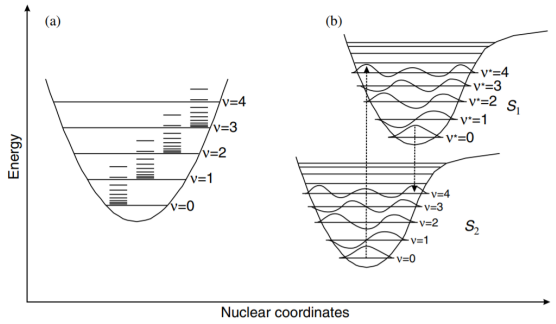

Figure 2.1: Franc-Condon Principle. The figure has been taken from *Handbook of Fluorescence Spectroscopy and Imaging* [5].

2.1.1 Conjugated bonds

An organic molecule with alternating single and double bondsis said to conjugated. This leads to a system where the π-electrons are delocalized from the double bonds and become mobile throughout the system. The reason for this is that all the carbons will have a π-electron 90° out from its σ-bonds, and the π orbitals will thus overlap over all the carbons in a conjugated chain. This leads to the possibility to assume the electrons as free particles in a box, which result in the common relation

$$\psi_n = \sqrt{\frac{2}{L} sin\left(\frac{n\pi x}{L}\right)} \tag{2.3}$$

and

$$E_n = \frac{n^2 h^2}{8mL^2} \tag{2.4}$$

where n is the quantum number, L is the length of the box, m is the mass, h is the Planck's constant and x is the x-coordintate. The length L is then the length of the conjugated system.

Each energy E_n correspond to a molecular π orbital, where there is room for two electrons. So if there are N electrons, the lowest N/2 energy levels would be filled. The

energy transition between the highest occupied molecular orbital (HOMO) and the lowest unoccupied molecular orbital (LUMO) then becomes:

$$\Delta E = \frac{h^2}{8mL^2}(N+1) \tag{2.5}$$

or alternatively

$$\lambda = \frac{8mcL^2}{h(N+1)}. \tag{2.6}$$

This is also called a $\pi \rightarrow \pi^*$ transition.

2.2 Emission of Light

After a molecule has absorbed a photon, the molecule will be in a new excited nonequilibrium state (Franck-Condon state). Only the fluorophore absorbed the energy and will therefore gain a dipole moment with a new orientation. The interaction between the new dipole of the fluorophore and the solvent is unstable, and some of the energy of the excited dye will be used to reorient the dipoles of the surrounding solvent. This is called (vibrational) relaxation [17].

If the solvent is polar, then a lot of energy is required to reorient their dipoles, and if the solvent is apolar, then the excited state will induce the dipole formation in the solvent, which requires less energy.

After the relaxation the excited molecule can then decay by emitting a photon. The emitted photon will thus have a longer wavelength than the absorbed photon, and this difference is called the Stokes shift. The more polar the environment is, the longer stokes shift becomes.

2.2.1 Donor-π-Acceptor transition

Another possible transition is the Donor-π-Acceptor. This is a type of photoinduced charge transfer, where a charge entity is transferred between two distinct atoms, functional groups or molecules after absorbing a photon [18]. The principles of the transition is demonstrated in figure 2.2. If a donor (D) is excited (D^*), it is then probable that the excited electron can decay to the acceptor (A). The absorption is also possible if the acceptor (A) is excited (A^*), as one of the electrons of the donor can ”fall down” to the acceptor.

2.3 Quantum yield

The quantum yield is a property of a fluorophore which denotes it’s probability to emit a photon after previously having absorbing a photon. A schematic representation of decay of a fluorophore is displayed in the Jablonski diagram in figure 2.3. First of all, if it is excited to a state higher than the first excited state, it will decay by vibrational relaxation and then internal conversion to the first excited state [5]. Internal conversion is also called radiationless de-excitation, and is the transition between a vibrational level in one electronic state to a vibrational level in a lower electronic state. This is probable when the vibrational

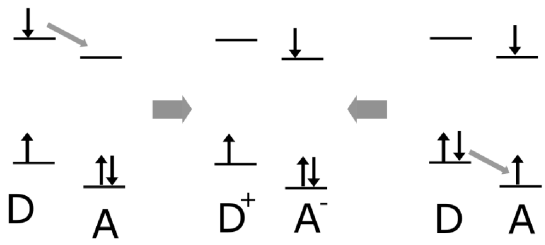

Figure 2.2: Donor-π-Acceptor transition.

energy levels strongly overlap electronic energy levels [19]. Most excitations thus end up in the lowest vibrational level of the first excited electronic state, $S_{1,\nu=0}$. The molecule can then decay to the ground state by internal conversion and vibrational excitation or by emitting a photon.

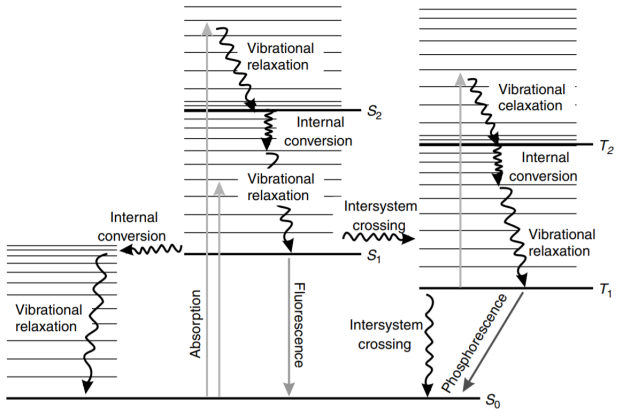

Figure 2.3: Jablonski diagram. The diagram has also been taken from *Handbook of Fluorescence Spectroscopy and Imaging* [5].

2.4 Phosphorescence

Phosphorescence is another type of decay that can take place by the reversal of the spin of an excited electron in what is called intersystem crossing. The molecule will then be in the first excited triplet state, instead of the first excited singlet state. The molecule can then decay by emitting a photon, which in this context is called phosphorescence. The reason for this is the longer lifetime of the triplet state (typically $10^{-6} - 10^{-1}s$ at room temperature) as opposed to the singlet state ($10^{-7} - 10^{-9}s$). The excited triplet can also again perform intersystem crossing to a vibrational level of the electronic singlet ground state. It can also absorb a new photon, be excited and then decay again to the first excited triplet state.

2.5 Excited state lifetime

The excited state lifetime is the average amount of time a fluorophore remains in an excited state after being excited [20]. The decay from an excited state is a random event, which means that it can be described as exponential decay. Thus the probability of a fluorophore to be in an excited state at time t is given by

$$P(t) = e^{-t/\tau_0}, \tag{2.7}$$

where τ_0 is the lifetime of the excited state [20].

By looking at a large number of excited molecules at $t = 0$, N_F^0, the number of excited molecules at time t becomes [3]

$$N_f = N_F^0 \cdot e^{-t/\tau_0}. \tag{2.8}$$

Measured in measured intensity I of the emitted photons the equation becomes what is called the theoretical response function:

$$I(t) = I_0 e^{-t/\tau_0} \tag{2.9}$$

where I_0 is the intensity at $t = 0$ [20].

2.6 Two-photon absorption

A fluorophore can normally not be excited by a photon with energy lower than the energy gap between the ground state and the first excited state. However, at high intensities, it becomes more probable for two photons to instantaneous combine their energy and excite a molecule. The photons can have different energy, but the sum must match the energy difference between the states.

The selection rules for one-photon absorption (OPA) and two-photon absorption (TPA) are different. The reason for this that photons have a spin of ± 1, so absorption of one photon result in an electron changing its molecular orbital to on with an angular momentum changed by ± 1. Two-photon absorption would require a change of ± 2 or 0. A fluorophore can therefore not be excited to the same state by OPA and TPA (this holds for "pure" states).

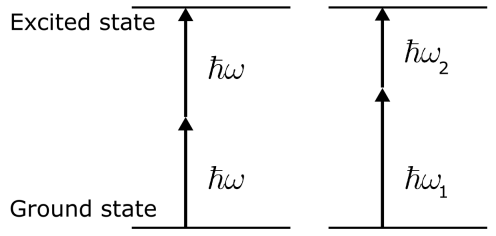

Figure 2.4: Two-photon absorption.

Chapter 3

Introduction to Amyolid Fibrils

3.1 Protein folding and misfolding

Proteins need to have the correct three-dimensional fold, the so-called native conformation, to operate correctly in the body. There are millions of theoretically possible folds, where each fold will have a different free energy and also different properties within the cell [6].

The energy landscape of the folding process is often described as a funnel, which is illustrated in figure 3.1a. Initially, a new protein is located near the top of the funnel, where there is high energy and large degree of conformational freedom, i.e. entropy. The protein then travels to low energy and stable conformation at the bottom, where it reaches the lowest free energy state, which is the native confirmation in the majority of cases [21]. The native fold is usually the most energetically favourable state and also the most probable.

There are numerous cellular structures within a cell and so, when a protein folds, it is surrounded by other proteins. This enhances the risk of making inappropriate contacts with other proteins or becoming partially misfolded [21]. Mutations, changes in the environmental conditions or chemical modifications can also cause misfolding [22].

Misfolded proteins are prone to aggregate and can, as previously mentioned, result in several human diseases. The largest group of misfolding diseases, in number of patients, is associated with the conversion of proteins into highly organized fibrillar aggregates. These generally described as amyloid fibrils [8].

3.2 Amyloids

An amyloid fibril protein is currently defined as such, if it deposits as insoluble fibril, mainly in the extracellular spaces of tissues and organs. Additionally, the amyloid fibril must bind to Congo red and exhibit green, yellow or orange birefringence when viewed in polarized light [23]. However this has recently been challenged [24, 25]. The amyloid structure will also have a β-rich conformation [9].

Amyloid deposits are primarily composed of a single protein [9] and the fibrils usually

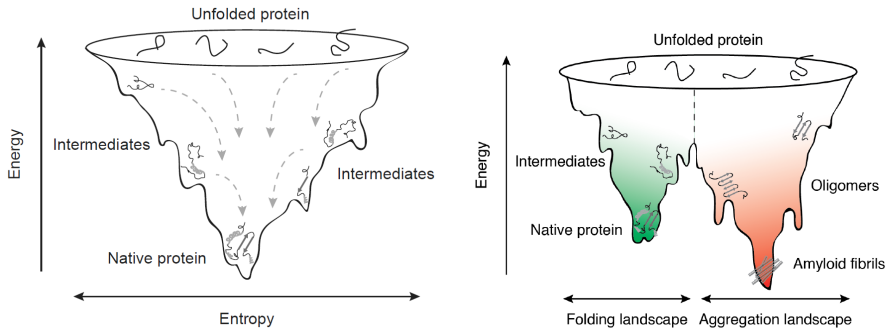

Figure 3.1: Schematic showing folding pathways for amyloid and non-amyloid proteins. Figures from Maria Jonson's doctorate [6].

consist of a between 2-6 protofilaments, where each is about 25 nm in diameter, and will form ropelike fibrils which are 7-13 nm wide [26] or form ribbons that are 25 nm thick and up to 30 nm wide [27].

The structure of an amyloid fibril is of low free energy and can thus be an alternative to the native state of a protein. An extended version of the folding landscape can be described as in figure 3.1b. The protein can be more stable in the amyloid state than in the native state, usually as a consequence of a critical concentration or differences in pH. However, as long as there are high free energy barriers that hinder the transition into the more stable amyloid state from the native state, then the native state can still persist [6].

3.3 Binding

The fluorescent probes can attach covalently or noncovalently to the structures of interest. The probes screened in this document are of the latter kind usually used for detection of amyloid fibrils [28].

3.3.1 Binding affinity

Binding affinity is the strength of the binding between a biomolecule – such as a protein – and a ligand/probe. It is usually measured by the equilibrium dissociation constant K_D, which is given by

$$K_D = \frac{[P][L]}{[PL]}. \tag{3.1}$$

Here [P] and [L] is the concentrations of respectively proteins and ligands, and [PL] is the concentration of the protein-ligand complex. K_D is thus inversely related to the binding; so a smaller K_D value implies a more efficient binding.

3.3.2 Why does fluorescence increase upon binding?

The binding site of a probe is usually to a hydrophobic pocket, and in this hydrophobic environment there are usually less polar groups that can quench fluorescence.

The dye imposes steric hindrance from the binding site, which may cause overlapping electron clouds. This can make certain conformations, such as extended π-conjugation, more favourable [29]. An increased transition dipole moment that follows an extended conjugated chain, gives stronger fluorescence.

3.4 Insulin structure

Native insulin has a structure of two short polypeptide chains constrained by one intramolecular and two intermolecular disulfide bonds [30]. The structure has a predominantly α-helical structure and is illustrated in figure 3.2.

Fibrillar insulin has a β-sheet rich conformation. The structure of the β-sheet within the fibril has not been settled, and has been proposed to be parallel, anti-parallel and also flat [30].

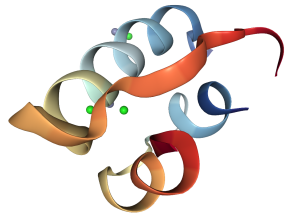

Figure 3.2: Structure of native insulin. Figure taken from the Protein Data Bank [7].

Chapter 4

Methodology

4.1 Methods of Optical Spectroscopy

4.1.1 Samples and blanks

The dye is first placed in a cuvette along with an appropriate solvent. This will be referred to as a sample. The cuvette and the solvent should be as transparent as possible, to minimize its affect to the measurement. There will still be some influence however, and therefore, a cuvette containing only solvent, called a blank, is also measured.

4.1.2 Absorption Spectroscopy

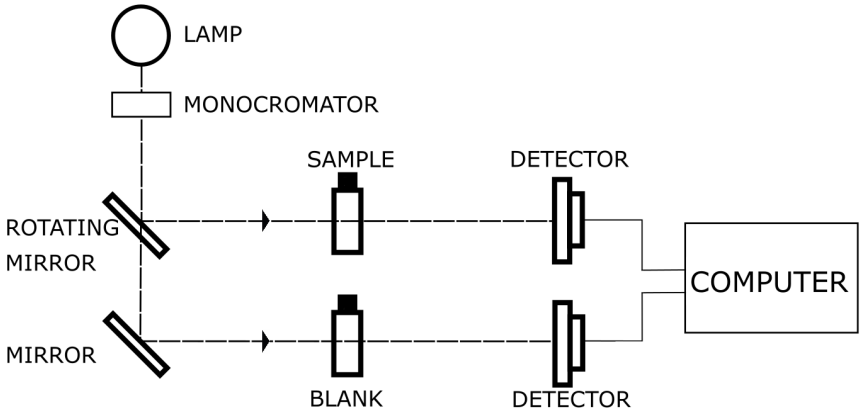

Figure 4.1: Principle of two-beam absorption measurement.

A schematic representation of the absorption measurement is shown in figure 4.1. The light from the lamp passes through the monocromator, which transmits only determined

wavelengths. A rotating mirror essentially splits the light into two paths: one through the sample and one through the blank. The absorption is then measured by the comparing the intensity of the light passing through the sample, I, and through the blank, I_0, as per Beer-Lamberts law in equation 2.2. This is done for each wavelength of interest, and the result is a graph with the absorption plotted against the wavelength.

First, a baseline should be measured to improve the accuracy of the result. A baseline is a calibration of the machine where it contains two blanks. The reason for this is that the two pathways of the light may vary from each other and it is necessary to define zero absorption over the desired wavelength range.

The measurements were were carried out using a Shimadzu UV-Vis Spectrophotometer, Model UV-1601PC.

4.1.3 Emission of light

The principle setup of a fluorescence measurement is displayed in figure 4.2. A lamp and a monocromator is used to excite the sample with light of a single wavelength. Alternatively, a laser with well defined wavelength can be used. The excitation wavelength is chosen from the absorption measurement.

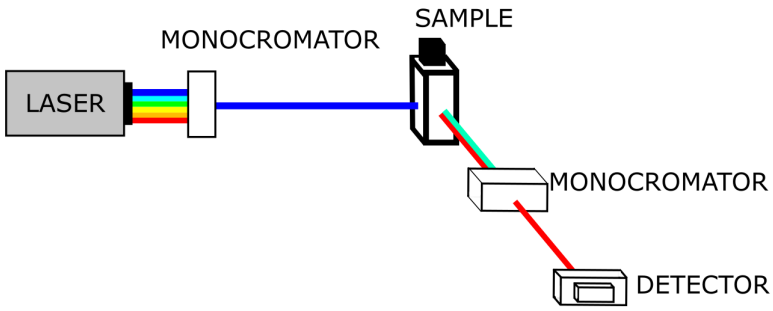

Figure 4.2: Principle of emission measurement.

The fluorophore can then emit light as is decays (see ch. 2.2). A monocromator in front of the detector screens the wavelength so that the the quantity of emitted light at the different wavelengths can be measured. The result is a graph with the measured quantity of photons plotted against emitted wavelength.

The cuvette and the solvent will again affect the result and therefore the measurement is also carried out with a blank. The emission from the blank is then subtracted from the emission of the sample.

The measurements were performed on a PTI QuantaMaster 8000 Series Fluorometer.

4.1.4 Quantum yield

There are two methods for calculating the quantum yield: the absolute determination and the relative determination. The relative method requires another sample with a known

quantum yield and is usually the preferred alternative because it is the easiest and probably also the most reliable [3]. The essence of the method is to compare the linear relation of the absorption and fluorescence for the known and the unknown sample. This is expressed by the equation

$$\frac{\Phi_S}{\Phi_{Ref}} = \frac{\Delta F_S/\Delta A_S}{\Delta F_{Ref}/\Delta A_{Ref}} \left(\frac{n_S}{n_{ref}}\right)^2 = \frac{a_S}{a_{ref}} \left(\frac{n_S}{n_{ref}}\right)^2 \tag{4.1}$$

where Φ are the quantum yields, F and A are the measured fluorescence and absorptions, a are the calculated linear relations and n are the refractive indexes [3].

The absorption and the fluorescence are measured for different concentrations to gain the required linear relation. To gain an accurate result, it is vital that the experimental circumstances changes as little as possible during the measurements. All the connected measurements should therefore be calculated with the same settings and within as a small time-frame as possible. It is not important to know the exact concentration of the each sample, as long as the fluorescence and absorption are measured with the same sample.

The error of the quantum yield calculation becomes, as per the Gaussian equation [31],

$$\begin{aligned}\left(\frac{\Delta\Phi_s}{\Phi_s}\right)^2 = &\left(\frac{\Delta\Phi_{ref}}{\Phi_{ref}}\right)^2 + \left(\frac{\Delta a_s}{a_s}\right)^2 + \left(\frac{\Delta a_{ref}}{a_{ref}}\right)^2 \\ &+ 4\left(\frac{\Delta n_s}{n_s}\right)^2 + 4\left(\frac{\Delta n_{ref}}{n_{ref}}\right)^2.\end{aligned} \tag{4.2}$$

4.1.5 Excited state lifetime

The excited state lifetime is usually measured using Time-Correlated Single Photon Counting (TCSPC). The instrumentation schematic is show in figure 4.4.

Pulsed light from the light source passes first through a monocromator and excites the sample. The emission passes through another monocromator and is then detected. The second monocromater reduces the measurement noise.

The time from the excitation to the detection of emission is measured by a time-to-amplitude converter (TAC). When the excitation pulse is emitted, it also sends a TAC start signal. This triggers the charging of a capacitor in the TAC, which increases the voltage gradually. The first photon that hits the detector will then send a TAC stop signal which results in an output pulse whose voltage is then converted to a time channel by a multi-channel analyzer [20]. The TAC resets if no photon hits the detector within a set reasonable timeframe. The experiment is usually continued until more than 10,000 counts has been collected in the peak channel.

A restriction set upon the measurement is that only 1 $\%$ of the pulses should result in a detected photon. The reason for this is that only after the first photon is detected, the dead-time of the detector prevents the detection of another photon from the same excitation pulse. If many photons is emitted towards the detector with each pulse, then the measured lifetime would be distorted to shorter times. The restriction solves this.

It may also be necessary to record the instrumental response function (prompt) of the pulse, as it can not be considered as a δ-function when the lifetimes are short [20]. The prompt is measured by setting the monocromators to the excitation wavelength and using

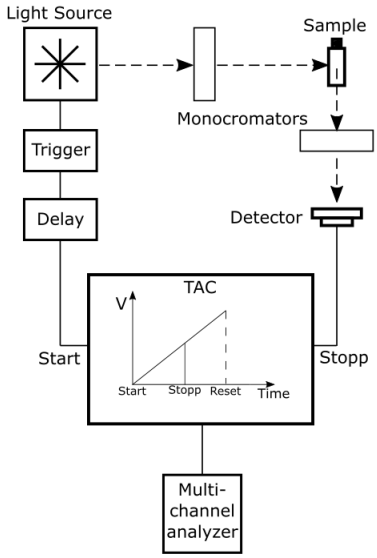

Figure 4.3: Principle of the TCSPC-setup.

a sample of ludox to scatter the light. The measured prompt can then be interpreted as a series of δ-fuctions, each creating an impulse response function $I(t, \tau)$ proportional to the height of the prompt. The theoretical response function was given in equation 2.9. The sum of these is the measured decay. In other words the fit F of the measured data is the convolution of the theoretical response function $I(t, \tau)$ and the prompt $P(t)$ and becomes

$$F(t) = \int_0^t P(t')I(t - t', \tau)dt'. \tag{4.3}$$

The lifetime(s) τ can then be calculated.

4.1.6 Two-photon Excited Fluorescence

The determination of the two-photon cross section is a relative technique and requires a reference sample with known two-photon cross section. It is also necessary to know the quantum efficiency of both the sample and the reference.

The essence of the method is to illuminate the sample with a high intensity laser beam and then measure the emitted fluorescence. It is then possible to use the quantum efficiency to acquire an estimate of how many molecules were excited. The next step is then to compare the sample and the reference, making sure to including possible differences in concentration and indexes of refraction. The two-photon cross section of the sample, $\sigma_{2,s}$, can then be calculated by

$$\sigma_{2,s}(\lambda) = \frac{\langle F(t)\rangle_s}{\langle F(t)\rangle_r} \cdot \frac{\Phi_s c_s n_s}{\Phi_r c_r n_r} \cdot \sigma_{2,r}, \tag{4.4}$$

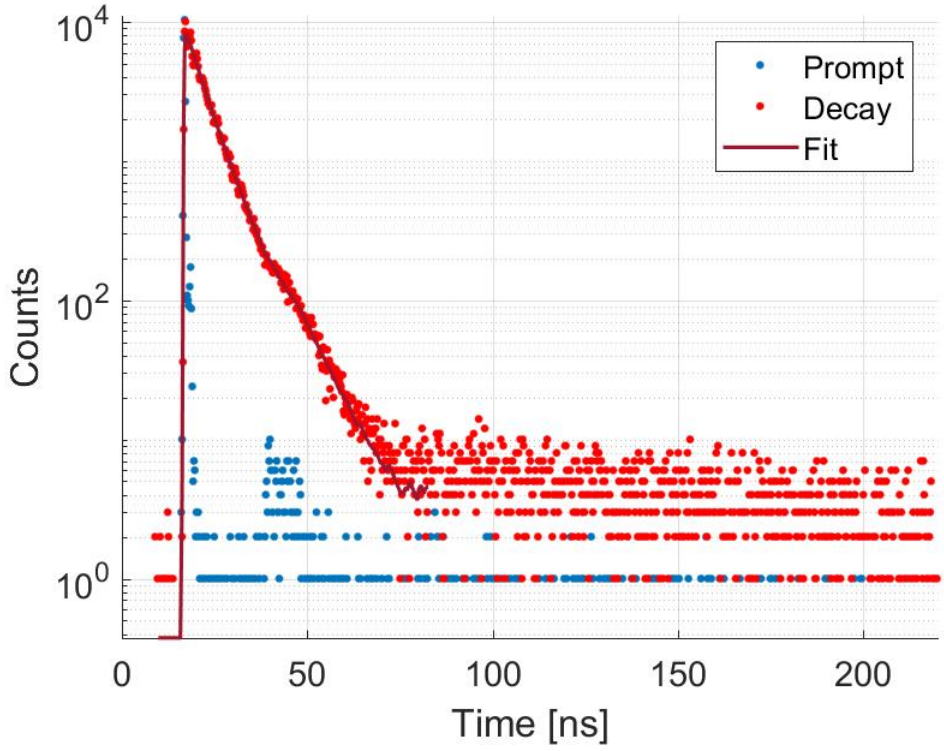

Figure 4.4: Graph showing the measurement of lifetime using TCSPC.

where $\langle F(t) \rangle$ is average detected fluorescence, Φ is quantum efficiency, c is concentration and n is index of refraction [3].

A schematic representation of the setup is shown in figure 4.5. Laser light from the Ti:Sapphire laser passes through the pulse picker, which picks one in 16, giving a pulse repetition frequency (prf) of 4.75 MHz. The sample is thus illuminated by pulses of around 50 mW, which should be enough intensity for multi-photon excitation, as each pulse is approximately 180 - 200 fs long. A detector is placed $90°$ in relation to the incident light path.

4.2 Methods of Fibrillar Fluorescence

4.2.1 Native and fibrillar proteins

A solution of native proteins can relatively easily be made by adding proteins in an appropriate solvent. The solvent must be chosen to make the proteins stable in their native confirmation. Later the solution may need to be put into an ultrasonic bath if the concentration is too high.

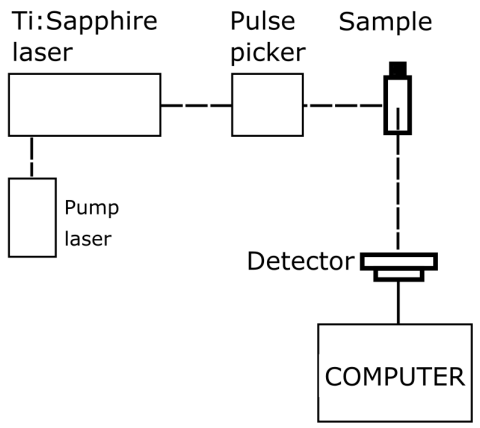

Figure 4.5: Setup for the measurement of TPA.

To make make a fibrillar proteins from the solution of native proteins, it is necessary to overcome the barrier keeping the proteins in the native state. If this is an energy barrier then simply heating the sample can be enough. This is illustrated in figure 3.1b, where by increasing the energy the proteins can move up in the funnel to where there is more entropy and they can then move above the second (amyloid) funnel. There are usually more possible configurations above this funnel, so it is probable that the proteins will stay there when cooled.

An example of of this type of change is the boiling of an egg, where the energy from the water changes the proteins into different confirmation. The egg stays in the new confirmation when cooled.

4.2.2 Measurement of the emission on a fluorescence plate reader

The fluorescence were measured with a fluorescence spectroscopy plate reader. This allows a large number of samples to be measured at roughly the same time. The plate consist of a series of wells, which was filled with $300\mu L$ of solution, and this means that there are room for errors in concentration. This is not a vital problem during a screening process.

The fluorescence is measured by first exciting the sample from below with an appropriate wavelength, and then measure the wavelength and intensity of photons emitted above. The principle is illustrated in figure 4.6.

4.2.3 Measuring the binding affinity

The binding affinity was measured using the plate reader. The concentration of the dye is kept constant in a series of wells while the concentration of the proteins is varied. It is then possible to plot the concentration of dye versus the emitted fluorescence. An example can be seen in figure 4.7, which show the binding of insulin in native and fibrils conformation to the dye BTD-3. At some point all the binding sites of the proteins will be saturated, and

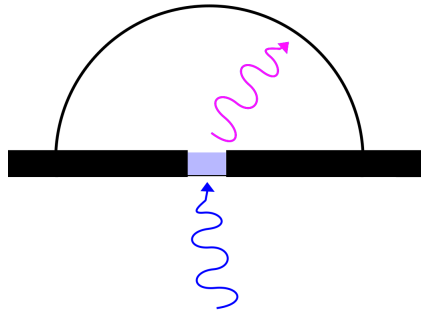

Figure 4.6: Fluorescent measurement with the plate reader. The light is measured by an integrating sphere above.

the emitted fluorescence of the sample will not increase. The K_d value can be found by finding the ligand concentration at half the fluorescence value of this [32].

In figure 4.7 it appears that native insulin is approximately saturated, but that fibrillar insulin should be measured for higher concentrations.

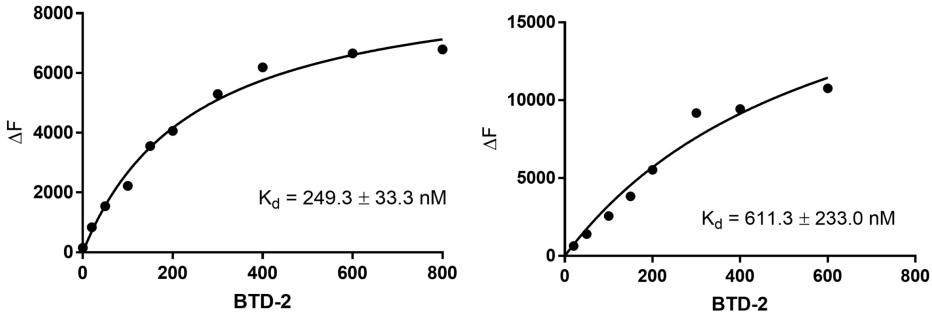

(a) Native insulin with BTD-2.

(b) Fibrillar insulin with BTD-2.

Figure 4.7: Binding curves of BTD-2 with native and fibrillar insulin.

4.3 Microscopy Techniques

4.3.1 Microscopy slides

A drop of the sample solution along with a drop of stabilizing solution is placed in the middle of a flat glass slide. A cover slip, which is a very thin square piece of glass, is placed on top of the glass slide, and the slides are then ready for microscopy. The slides can be sealed if they need to be kept for a longer period of time.

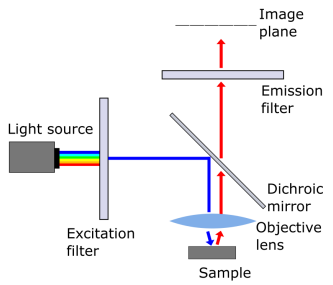

Figure 4.8: Schematic setup of fluorescence microscopy.

4.3.2 Fluorescence Microscopy

A schematic setup for a fluorescent microscope is shown in figure 4.8. Photons from the light source will first go through the excitation filter, which only transmits light of a determined wavelength. Since different molecules usually absorbs different wavelengths of light, it is then possible to decide which fluorescent dyes are to be excited if more than one are present.

Next is the dichroic mirror, which will reflect or transmit light depending on the wavelength. Usually it will reflect photons below a certain wavelength and transmits above another or the same wavelength.The short wavelength light will be reflected by the mirror and hit the sample and fluorescent light will be emitted. This light will then pass through the dichoric mirror, as it has a longer wavelength, and hit the emission filter. This filter will only transmit wavelength matching the fluorescent emission and thus prevent unwanted wavelengths from disturbing the resulting image. A colourful image can be formed by using multiple fluorescent dyes, all marking different structures in a sample, and then combining the images.

4.3.3 Confocal and Multi-photon Microscopy

The fluorescent microscope will excite molecules throughout the entire depth of the sample, and not only in the objective lens' plane of focus. The resulting image will thus appear blurred. The image becomes sharper by employing a confocal microscope, which is able to produce an image plane by plane, and thus the result will be more focused.

The confocal microscope is quite similar to the fluorescent microscope described so far. The main difference in the structure is the presence of a scanning mirror, shown in figure 4.9, which determines the spot to be examined. The beam can then be swept over the specimen in a precise pattern, aquiring data from each spot. The detector collects this data and then digitises and display the complete image. Fluorescent emission from other planes still take place, but those photons will hit the pinhole and not the detector.

Even though the result will be sharper, the light above and below the chosen plane is continuously being excited. This can result in a rapid bleaching of the fluorescent molecules [10]. This is especially true for biological material, as it is quite often fragile. This can be avoided however, by the use of multi-photon excitation microscopy, in which light with a higher wavelength is used. The principle is: in planes below and above the chosen focus,

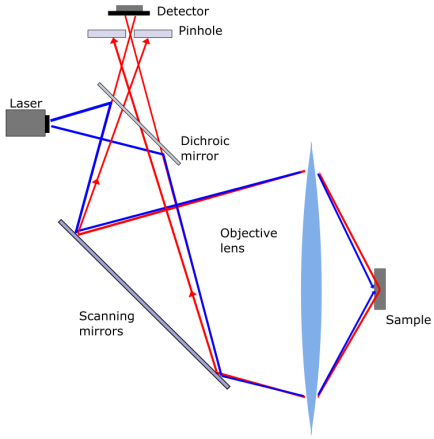

Figure 4.9: Schematic of confocal microscopy.

the light has to little energy to excite anything, but in the focus plane, two photons may combine to effectively approximate a photon with more energy. Only the focused spot in the chosen plane is thus excited.

Chapter 5

Experimental Results and Discussion

5.1 Spectroscopic characterisation

A series of samples was provided in the collaboration project with Linköping University. Our main task was to carry out advanced optical spectroscopy: absorption and fluorescence spectra, quantum yield, decay lifetimes and two-photon absorption cross section.

The measured absorptions and emissions are show in figure 5.1a, 5.1c, 5.2a and 5.2c. The samples all had the same concentration ($\frac{10^{-5}}{3}M$) and their solvent were toluene.

The exact detailed mechanisms and the exact quantum states occupied during the different excitations, emission, etc. would require substantial quantum chemical calculations. Especially since the molecules consist of several tens of atoms. This is beyond the scope of this thesis.

5.1.1 Absorption

The absorption peaks are all rather wide, which is reasonable considering that the molecules are composed of several tens of atoms, giving rise to many possible vibrations. In addition, the fluorescent dyes will interact with the solvent, furthering broadening the peaks. There are also conjugated chains in the molecules, which means that most of the vibrations are coupled to electronic transitions by the change in electron densities over the chains [5]. So the electron density changes after an electronic excitation, which is associated with a change in bond length. In terms of quantum mechanics this means that transitions have occurred from the electronic and vibrational ground state S_0 of the molecule to an electronically and vibrationally excited state S_1.

All the fluorescent dyes are conjugated, and therefore there should be many $\pi \rightarrow \pi^*$ transitions. It is probable that the peaks around 300-400 nm are all from this kind of transition.

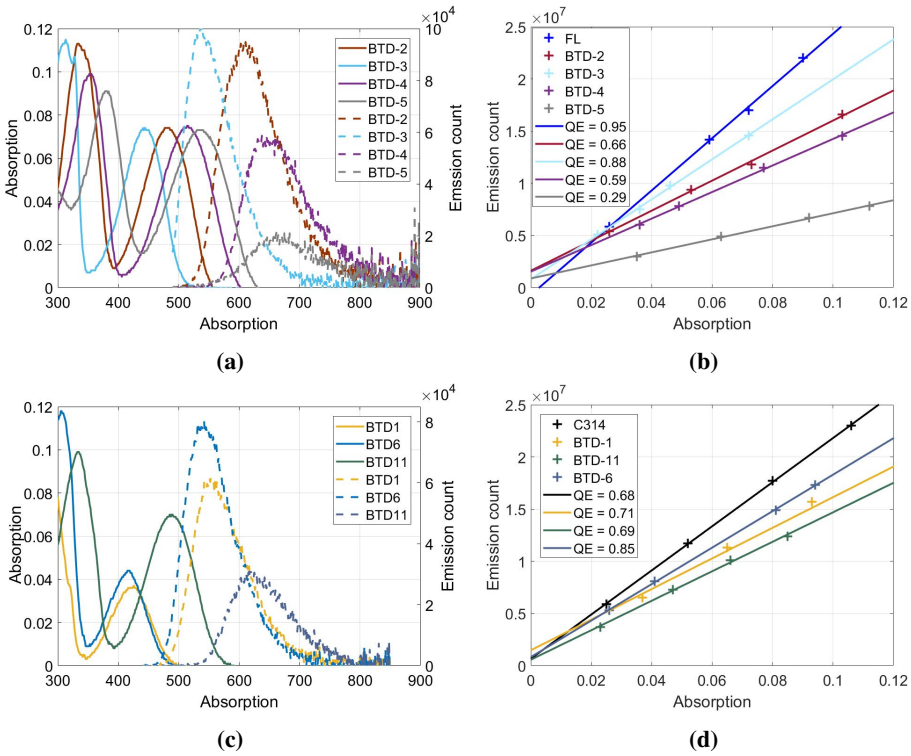

Figure 5.1: The absorption and emission spectra are show in a and c. The linear relation between absorption and emission is shown in b and d.

All the new dyes have a donor-π-acceptor-π-donor structure, where the OH-groups are the donors and the N-atoms are the acceptors. The second peaks are therefore probably from the charge transitions between these, as the absorption is located at a rather long wavelength [18]. This is supported by that DF-9, which does not have the 1,2,5-Thiadiazole-group, does not have a second peak above 400 nm.

The solvent chosen was toluene, which is a non-polar solvent. In a polar solvent like water it is expected that the absorption will require more energy and that the absorptions peaks will be red shifted. The reason for this is that the dipole-dipole interactions [17].

The extinction peak for the first peaks ε_1 does not vary significantly between the different samples. In addition the second peak ε_2 is always lower than the first peak ε_1. BTD-2 is a decent starting point for looking at the individual dyes, as it is similar to many of the others. It has the same structure as BTDSB except for that the COOH-groups have been removed. The effects of these can be seen in table 5.1. First of all this leads to a decrease of ε_1 and ε_2, which may be explained by the decrease in size. λ_{abs1} is red-shifted by only 3 nm, which is reasonable with that the length of the conjugated chain does not differ. However, λ_{abs2} is red-shifted 18 nm, which means that the COOH-group increased the energy gap between the donor and acceptor.

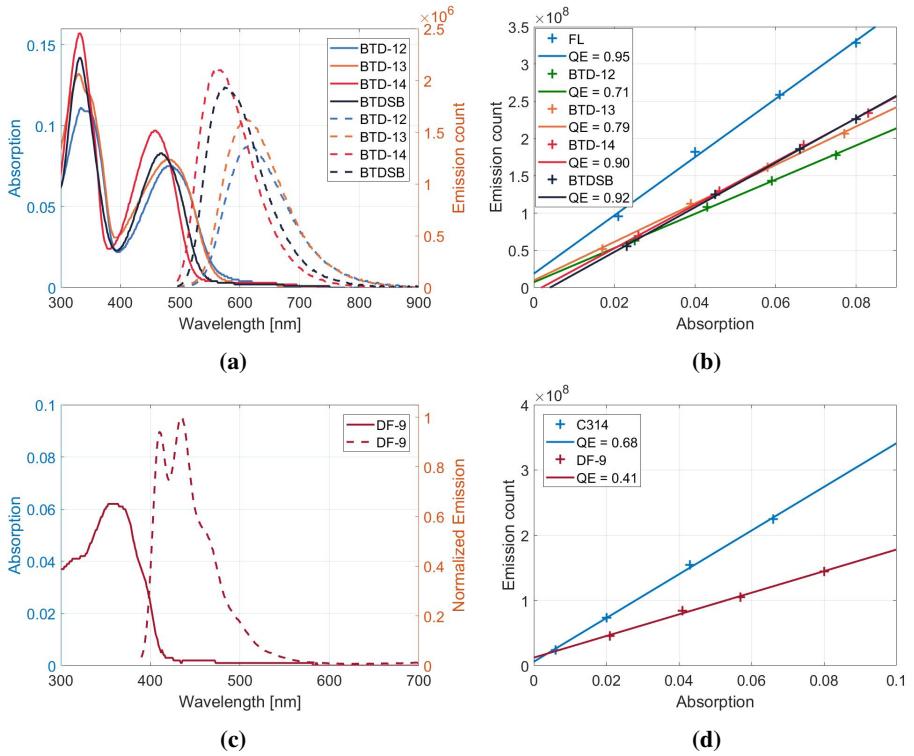

Figure 5.2: The absorption and emission spectra are show in a and c. The linear relation between absorption and emission is shown in b and d.

Sample	ε_{max1} $[(Mcm)^{-1}]$	λ_{abs1} $[nm]$	ε_{max2} $[(Mcm)^{-1}]$	λ_{abs2} $[nm]$	λ_{em} $[nm]$	Stokes shift $[nm]$	Quantum yield -
DF-9	18 600	354	-	-	435	81	0.41 ± 0.02
BTDSB	42 600	332	24 900	467	575	108	0.92 ± 0.04
BTD-1	$>$23 000	$<$300	11 100	426	554	128	0.71 ± 0.05
BTD-2	33 900	335	22 200	485	611	126	0.66 ± 0.03
BTD-3	34 500	313	22 200	445	538	93	0.88 ± 0.03
BTD-4	29 700	356	22 500	516	638	122	0.59 ± 0.02
BTD-5	27 300	384	21 900	541	662	121	0.29 ± 0.01
BTD-6	35 400	306	13 200	419	542	123	0.85 ± 0.02
BTD-11	29 700	335	21 000	490	616	126	0.69 ± 0.01
BTD-12	33 300	334	22 500	478	620	142	0.71 ± 0.03
BTD-13	39 600	330	23 700	476	611	135	0.79 ± 0.04
BTD-14	47 100	331	29 100	457	563	106	0.90 ± 0.04

Table 5.1: Summary of the photo-physical properties of DF-9, BTDSB and the new dyes in toluene.

BTD-1 has a shorter conjugated chain than BTD-2 and therefore λ_{abs1} has a peak at less than 300 nm. The exact placement of the peak is not known, as the absorption measurement is not accurate below 300 nm. The extinction coefficient ε_1 appears to be significantly lower for BTD-1, which again is reasonable considering the small size of the molecule. BTD-1 does not have a double bond between the benzene-rings and would therefore not have a rigid structure.

BTD-3 is interesting as it has a triple-bond between the benzene-groups. This means that there are more free electrons in the molecule and, according to equation 2.6, λ_{abs1} should be blue-shifted compared to BTD-2, which it is by 22 nm. λ_{abs2} is blue-shifted by 40 nm, probably because the HOMO is higher.

The double-bond in BTD-2 is replaced by tiofen in BTD-4. This leads to an extension of the conjugated chain and thus a red-shift of λ_{abs1} by 21 nm. This can also be seen in BTD-5 where the chain is further extended by double-bonds and a red-shift of 49 nm is instead measured. ε_1 is smaller for BTD-4 and BTD-5 than in BTD-2, so the added tiofen makes the probability of absorption of a photons smaller. This can be an effect of less planar structure. ε_2 is not significantly affected by the tiofen, but λ_{abs2} becomes red-shifted by respectively 31 nm and 56 nm for BTD-4 and BTD-5.

In BTD-6 the double-bond in BTD-2 is replaced by another benzene ring. This distorts the conjugated chain and the λ_{abs1} is blue-shifted 29 nm and also increases ε_1. However, this decreases ε_2 significantly, probably because it is more difficult to transfer the charge with the distorted chain and because the dye loses it's rigidity. The molecule loses it rigidity because all the carbon atoms in the benzene rings contain a proton, which will repulse each other. Therefore it has no planarity.

BTD-11 is similar to the BTD-4, where a benzene ring with a OH-group has been removed. This also means that the molecule is no longer symmetric and has a donor-π-acceptor-π structure. First of all, the conjugated chain becomes shorter so λ_{abs1} is blue-shifted 21 nm, but ε_1 is unchanged. λ_{abs1} is blue-shifted 26 nm and ε_1 only decreases slightly.

BTD-12 has the same structure as BTDSB except that the COOH-groups are replaced by OH-groups. λ_{abs1} is not significantly affected by this and λ_{abs2} is red-shifted 11 nm.

BTD-13 and BTD-14 demonstrates the consequences of the removal of OH-groups. λ_{abs1} is not significantly changed by this, but λ_{abs2} is blue-shifted 2 nm and then 21 nm relative to BTD-12. Interestingly ε_1 and ε_2 increase with the removal of OH-groups.

BTD-2 and BTD-14 has their two OH-groups located at different places in their structure. ε_1 is ca 40 higher for BTD-14 but λ_{abs1} is more or less the same. ε_2 also increases, this time by ca 30 and λ_{abs2} is blue-shifted 29 nm.

5.1.2 Emission

The fluorescence spectra are all wide, much for the same reasons as for the absorption spectra. Their emission maximum λ_{em} and stokes shift are given in table 5.1. These were all measured from λ_{abs2} (except for DF-9 which was measured from λ_{abs1}). In principle the emission occurs from the excited state independently of the excitation wavelength [17], but since there are two different mechanisms of absorption there may be some differences between absorption through the λ_{abs1}-peak and the λ_{abs2}-peak. However, this was not investigated.

The stokes shift for most of the dyes are located around 120-130 nm. The exceptions are DF-9, BTDSB, BTD-3, BTD-12, BTD-13 and BTD-14. The different molecules will of course have different possible energy states and there will also be differences in the vibrational energy lost to surrounding solvent during the relaxation to the $S_{1,\nu_{=0}}$-state [33], as the different molecular structures will interact different with the solvent. The energy gap between the donor and acceptor will also vary.

From examining the results of BTD-2, BTD-12, BTD-13 and BTD-14, it is possible to see a trend from effect of the OH-groups. BTD-12 has the longest stokes shift and BTD-14 has the shortest, so it appears that fewer OH-groups leads to shorter stokes shift. Between BTD-2 and 14 only the placement of the OH-groups is different, and the difference in stokes shift is 20 nm, which is significant. It would be necessary to carry out quantum chemical calculations to obtain more detailed information of the participating electronic states.

5.1.3 Quantum yield

The measured quantum yields of DF-9 and BTDSB and it's derivatives in toluene are given in table 5.1. The references for 2 to 5, 12 to 14 and BTDSB were fluorescein in NaOH [34] whereas C314 in ethanol [35] was used for the rest. The dyes were excited at respectively 475 nm and 440 nm, except for DF-9, which was excited at 375 nm.

All the quantum yields are quite high, which is partially a consequence of using toluene as the solvent. Toluene is a non-polar solvent which often result in a high quantum yield [33] and was used because it gives a good model for comparison with amyloid binding sites. In a polar environment the intensity of emission will be lower [17] and thus the quantum yield will also be lower.

Again, it is interesting to look at BTD-12, BTD-13 and BTD-14 to look at the influence of the OH-groups. The quantum yiled rises sharply as the OH-groups are removed, but this not hold water compared to BTD-2. BTD-2 has also only two OH-groups and yet has a lower quantum yield that than BTD-12, which has four. This suggest that the location of the OH-groups has a large effect on the quantum yield.

BTD-4, BTD-5 and BTD-11 all have tiofen groups in their molecule and are among the four with the lowest quantum yield. The fourth member is DF-9. This suggest that the added group increases the vibrational states of the dye, and thus the probability for internal conversions.

Excluding DF-9, a general trend can be seen in that with increasing λ_{em} the quantum yield decreases. The reason for this is may be that there are more radiationless transitions at longer wavelengths due to vibrational overlaps between the ground and excited states [36]. This can also be the explanation for the low quantum yield of the dyes with tiofen-groups, since they all have long λ_{em}.

5.1.4 Lifetimes

The lifetimes are displayed in table 5.2. All the new samples have relatively long lifetimes (τ_{gave}>4 ns), which may be a result of their rigid structures, since rotation around double bonds contributes to a decrease in lifetime [36].

Many of the molecules have two lifetimes, which may be explained by the decay to different vibrational states of the ground state. It can also be explained by the orientation of the dye in relation to the incoming light [37]. Again, the excat mechanism would require quantum chemical calculations.

The lifetime is affected by many factors, including temperature, polarity, refractive index, the presence of fluorescence quenchers, and even geometry [38]. Thus, the lifetimes are also dependent on the local environment, and can therefore be used for the purposes of Fluorescence lifetime imaging (FLIM).

All the new dyes have lifetimes in the nanosecond range and could therefore be possible candidates for fluorescence lifetime imaging (FLIM). This could be used for e.g. potentially detecting Alzheimer's disease amyloids [39, 11].

Sample	B_1	t_1	B_2	t_2	τ_{gave}	τ_{ave}
	$\%$	ns	$\%$	ns	ns	ns
DF-9	27	0.2 ± 0.07	73	0.9 ± 0.01	0.8	0.7
BTDSB	7	1.9 ± 0.8	93	5.9 ± 0.1	5.8	5.6
BTD-1	33	5.3 ± 0.2	67	10.3 ± 0.1	9.0	8.4
BTD-2	47	7.1 ± 0.1	53	3.9 ± 0.1	5.9	5.4
BTD-3	26	5.3 ± 0.1	74	2.7 ± 0.1	3.8	3.4
BTD-4	40	7.2 ± 0.1	60	4.2 ± 0.1	5.8	5.4
BTD-5	33	7.6 ± 0.2	67	2.4 ± 0.1	5.6	4.1
BTD-6	47	5.9 ± 0.1	53	3.0 ± 0.2	4.8	4.4
BTD-11	25	5.4 ± 0.7	75	8.0 ± 0.1	7.5	7.4
BTD-12	100	5.5 ± 0.1	0	–	5.5	5.5
BTD-13	100	5.8 ± 0.1	0	–	5.8	5.8
BTD-14	100	5.7 ± 0.1	0	–	5.7	5.7

Table 5.2: Lifetimes in Toluene. τ_{gave} is the geometric average.

5.1.5 Two-photon absorption cross-section

The two-photon absorption cross-sections at 750, 800 and 850 nm were measured and are given in figure 5.3 and table 5.3. The reference used was fluorescein [3].

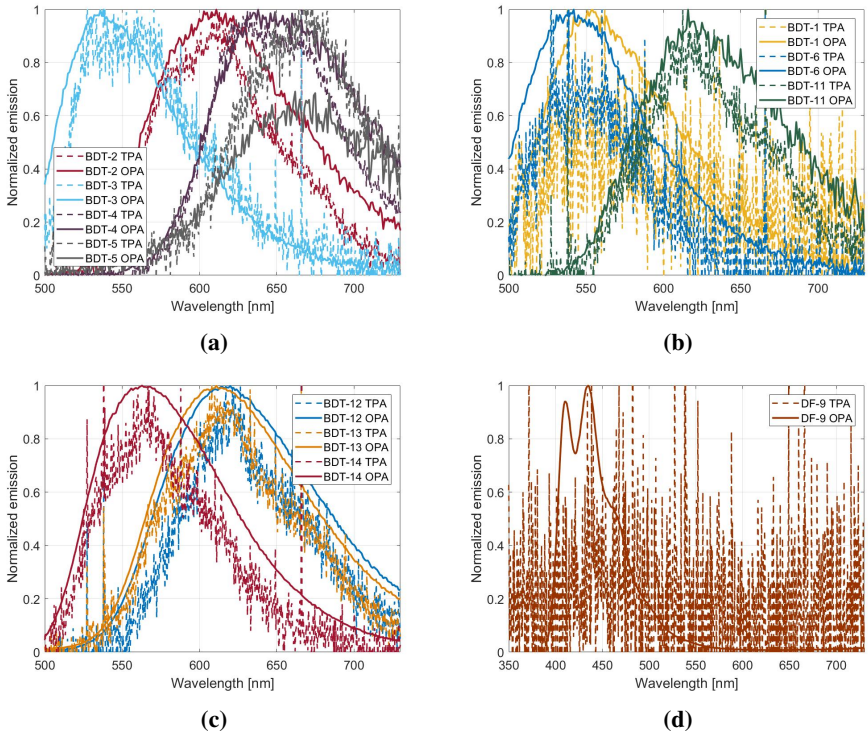

Figure 5.3: The plots compare the OPA (solid line) and the TPA (dashed line) emission spectra.

It is clear from results summarised in table that DF-9 does not have two-photon absorption properties. The reason for this may be a short lifetime of the excited state. A large TPA is also generally correlated with symmetric charge transfer within a conjugated system [40, 41], which DF-9 does not have.

The rest of the two-photon excited emission spectra are all practically identical to the one-photon emission spectra, however, this is difficult to determine precisely as the noise from the two-photon excited emission spectra is significant. It is still reasonable to conclude that the emissions originates from the same excited state because of the similarities. The reason for this is that, although the dye is excited to different states by OPA and TPA, the molecule will go through internal conversion to the same $S_{1,\nu_{=0}}$-state.

The TPA-values for many of the new dyes are higher than that of the reference fluorescein. The reason for this may be their symmetric charge transfer structure within a conjugated system. This can especially be seen in BTD-4 and BTD-5, which have the largest TPA. These molecules also have the longest conjugated chains separating the donors and acceptors. This generally results in large values for TPA [41]. This inference is also

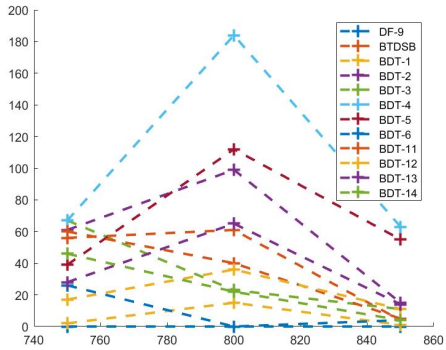

Figure 5.4: A figure

	750 nm	800 nm	850 nm1
Fluor	33	36	11
DF-9	<1	<1	<1
BTDSB	56	61	4
BTD-1	2	15	1
BTD-2	61	99	15
BTD-3	67	23	11
BTD-4	67	184	63
BTD-5	39	112	55
BTD-6	26	<1	4
BTD-11	60	40	5
BTD-12	17	36	11
BTD-13	28	65	14
BTD-14	46	22	4

Table 5.3: Two-photon absorption cross section.

supported by the low TPA of BTD-1 and BTD-6, which do not have long conjugated systems.

Interestingly BTD-11, which does not have a symmetrical structure, show a surprisingly large TPA. However, it is still much lower than the similar structure BTD-4, which illustrates the some of the effect from a symmetrical structure.

5.2 Fluorescence properties upon binding to insulin

The results of the measured fluorescence for native and fibrillar insulin in addition to a sample with only the probe is summarized in table 5.4. The solvent was water and all the samples were excited at their second absorption peaks λ_{abs2} (except for DF-9 and ThT which only has one peak). The effect of the solvent can be seen by comparing the emission peaks of the probe in water λ_{probe} as seen in table 5.4 and the probe in toluene λ_{em} as seen in table 5.1. All the peaks are red shifted in water compared to toluene, which is caused by the polarity of water.

BTD-6 and BTD-12 are both incapable to detect insulin fibrils, as the signal is more or less identical to the native signal. BTD-4, BTD-5 and BTD-13 only demonstrates a slight difference in emitted signal, and also has relatively low quantum yields. It is interesting that BTD-13 shows higher signal with native insulin, but this is not high enough to be of any significance. BTD-1, BTD-5 and BTD-11 show the largest increase in fluorescence, all between 80% and 90%, however they are all much lower than the two references, DF-9 and ThT, which increse with 1400% and 2800% respectively.

Sample	λ_{probe} nm	λ_{native} nm	λ_{fibril} nm	λ_f - λ_n nm	$\frac{\Sigma F_{fibril}}{\Sigma F_{native}}$ -	$\frac{\Sigma F_{fibril}}{\Sigma F_{probe}}$ -
DF-9	419	413	441	28	14.97	23.26
ThT	500	474	480	8	29.27	51.51
BTD-1	555	557	564	7	1.85	3.80
BTD-2	629	600	638	38	1.41	4.20
BTD-3	555	545	577	32	1.42	15.71
BTD-4	710	682	703	21	1.21	1.61
BTD-5	668	673	674	1	1.82	2.62
BTD-6	550	542	560	18	1.06	1.41
BTD-11	635	626	650	24	1.86	8.44
BTD-12	613	609	613	4	1.01	4.76
BTD-13	631	617	631	14	0.89	8.06
BTD-14	599	589	592	3	1.70	6.33

Table 5.4: The table displays the emission peaks native and fibrillar insulin with probe in addition to a blank sample with only the probe. ΣF is the sum of the emission.

However, many of the new dyes show a significant shift between the fibrillar, native and probe emissions. This is an interesting and possible useful property, and can be seen in BTD-2, BTD-3, BTD-11 and BTD-13.

There were not enough time to measure the binding curves of the the probes, other than that of BTD-3.

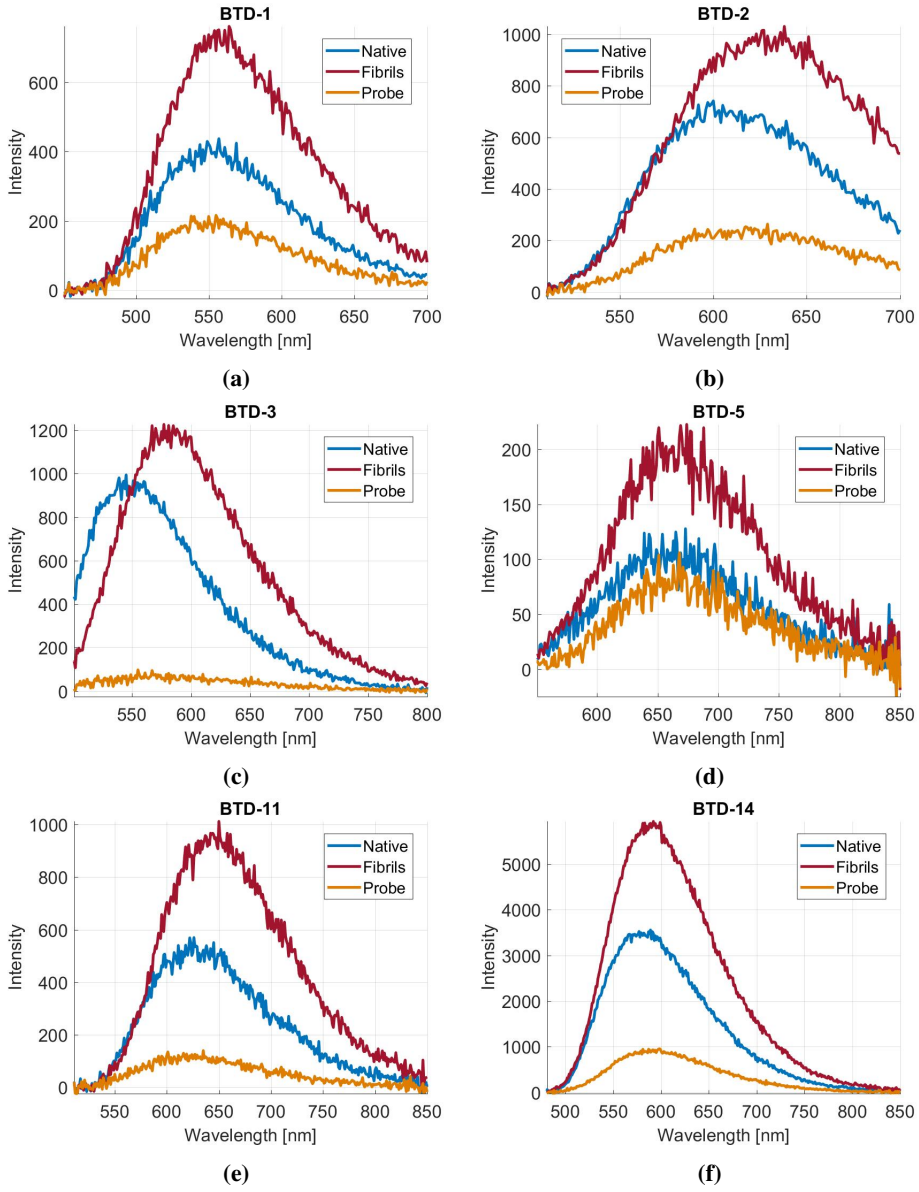

Figure 5.5: Emission spectra upon binding to fibrillar and native insulin.

5.3 Microscopy Images and spectra

Microscopy slides were prepared with the new dyes in fibrillar insulin and were subsequently tested in a confocal microscope with both OPA and TPA laser equipment. The resulting (monochrome) images from the most promising dyes are shown in figure 5.6. The samples contained only fibrils and so the formation of the amyloids are random and there is not much consistency between the pictures, except for that which was discussed in section 3.2.

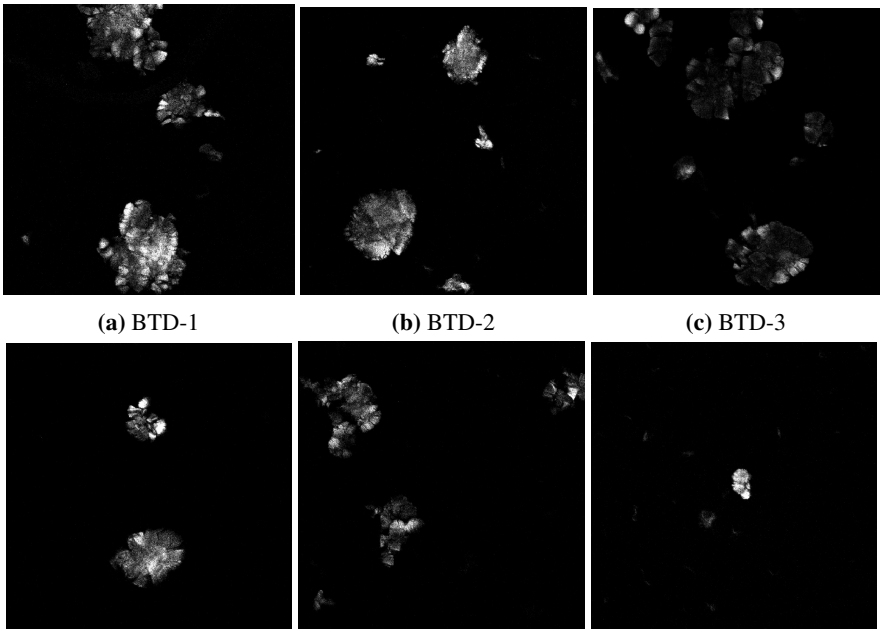

(a) BTD-1 **(b)** BTD-2 **(c)** BTD-3

(d) BTD-5 **(e)** BTD-11 **(f)** BTD-14

Figure 5.6: Pictures taken with a multi-photon microscope. The samples were excited with 800 nm.

The emission spectra from the centre of the fibrils are shown in figure 5.7 for OPA and TPA. All the plots matches eachother and those from figure 5.5 except for BTD-5, which show a shift of ca. 25-30 nm between the peaks in figure 5.7d. This is unexpected as the both should decay from the $S_{1,\nu=0}$-state, which should not change based with the excitation wavelength. It should be noted that the quantum yield for BTD-5 in toluene is only 0.29, which is very low, and it can be expected that it will be even lower in water, which is polar. To recieve a signal, the sample required high intensity light, which may have caused unknown effects. However, by comparing the peaks in 5.7d with the fibrils-peak in figure 5.5d, we can see that the peaks have a shift of 117 nm and 83 nm. Again, theoretically the peaks should be the same. This may be explained by noticing that BTD-5 is a long molecule (see figure 1.2e) and then hypothesise that BTD-5 in the amyloid state take on a confirmation with shorter conjugation length [42]. This would explain the movement of the peaks.

Figure 5.8 shows the emission spectra for the centre and the edge of the fibril formations.

BTD-14 (ex405) seem to show a slight difference, but nothing substantial. The reason for this may be the relatively low signal from the low exposure time or the decay of the samples.

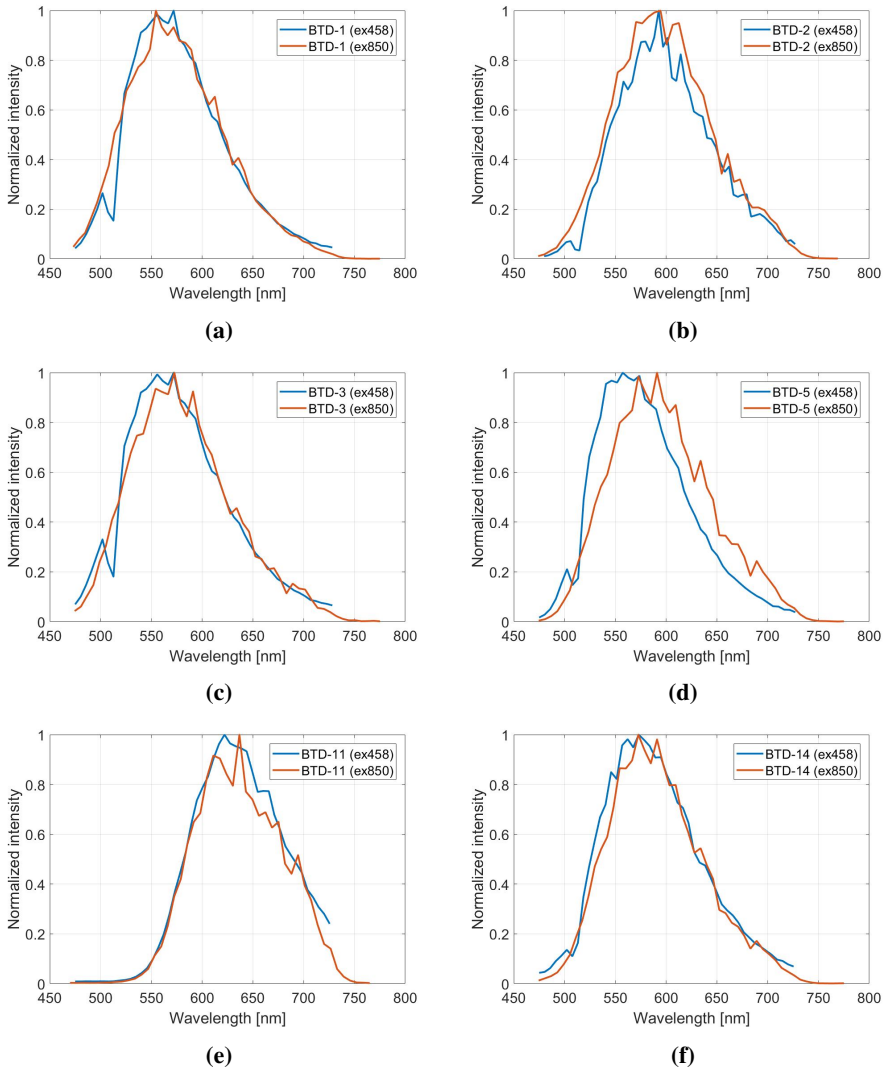

Figure 5.7: The graphs compare the emitted light from the OPA and TPA in the microscope.

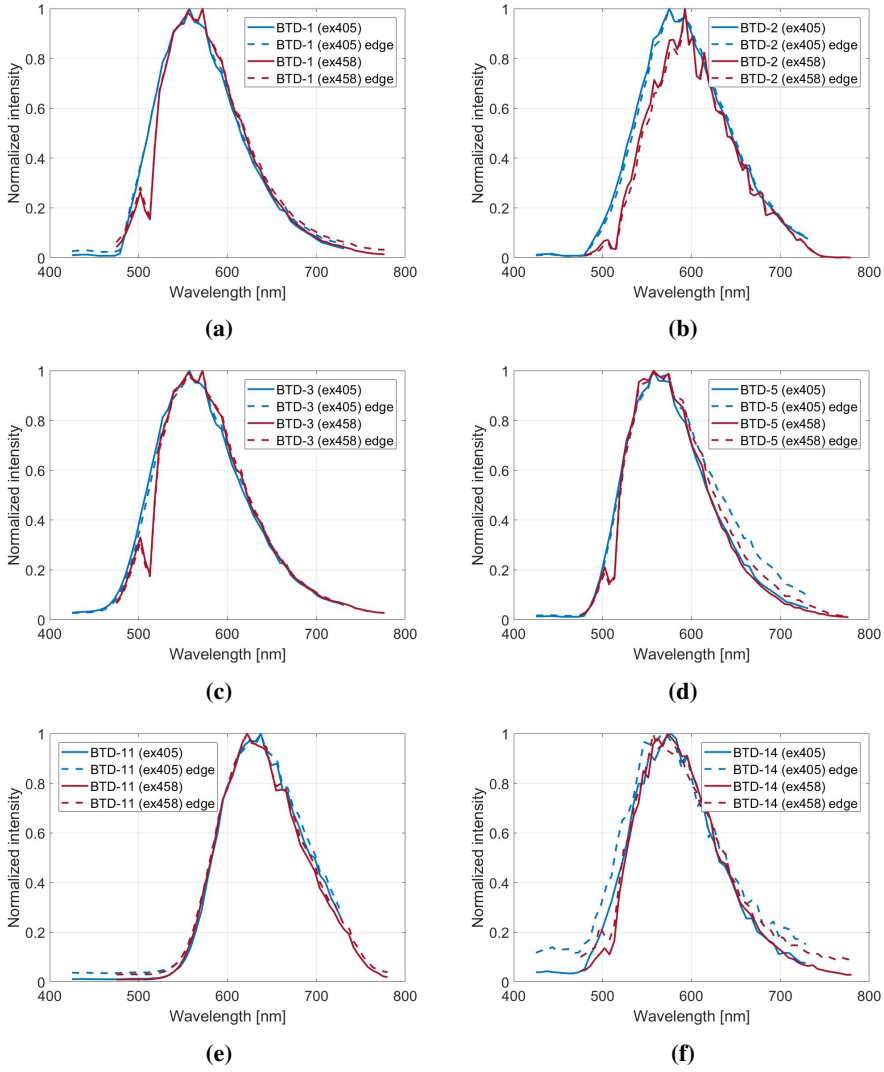

Figure 5.8: Comparison of the emitted light at the edges and the centre of the formations.

Chapter 6

Conclusion and Way Forward

All the new probes show fluorescent properties in a nonpolar enviroment. Most of the quantum yield are much higher than that of DF-9, and all the stokes shift are longer. This means that if the probes bind to a hydrophobic pocket in a otherwise polar environment (i.e. water) that quenches the probe, the new probe would be promising. To measure, or at least gain an estimate of, the quantum yields in a polar environment would therefore be interesting.

Six of the ten new samples showed higher TPA than the fluorescein, where BTD-4 and BTD-5 especially showed high values. However BTD-5 has generally a low quantum yield, and with the high intensity required for TPA it is probably not a applicable for multi-photon techniques. BTD-4 however, has a quantum yield twice as high and may be useful.

Not all of the new samples were able to differentiate between native and fibrillar insulin. BTD-1, BTD-5 and BTD-14 showed a significant increase in emission, but no large shift between the fibrillar and native peak. BTD-2 and BTD-3 showed a smaller increase in emitted light, but a longer shift. BTD-11 had an increase in emission equal to that of BTD-1 and also have a shift of 24 nm. However, none of the new samples come close to the increased fluorescence of DF-9 and ThT.

The new samples may still be of use for detection of insulin fibrils because of their high TPA. BTD-2, BTD-3, BTD-11 and BTD-14 may be used. BTD-5 can also probably be studied further, but it has, as mentioned, low quantum yield. BTD-11 has a decent quantum yield and TPA, and overall may be the most promising dye for detection insulin amyloid fibrils. BTD-14 is also promising, as it gives a strong signal.

Many of the samples has a decent basis for detection of amyloids and may be tested on different types of amyloids to test their affinity. In addition, it would be interesting to test the most promising molecules in FLIM experiments.

Bibliography

[1] B. A. Neto et al. "2,1,3-Benzothiadiazole and Derivatives: Synthesis, Properties, Reactions, and Applications in Light Technology of Small Molecules". *Eur. J. of Org, Chem,*, 2013(2):228–255, 2018.

[2] J. Zhang et al. "Detection and Imaging of A−42 and Tau Fibrils by Redesigned Fluorescent X-34 Analogues". *Chemistry*, 35(28):93–98, Mar 2008.

[3] E. Glimsdal. *Spectroscopic characterization of some platinum acetylide molecules for optical power limiting applications*. Aug 2009. PhD thesis.

[4] Inc. eMolecules. Visited 18.11.2017 `https://www.emolecules.com/`.

[5] M. Sauer et al. *Basic Principles of Fluorescence Spectroscopy, in Handbook of Fluorescence Spectroscopy and Imaging*. Wiley-VCH Verlag GmbH Co., 2011.

[6] M. Jonson. *Investigating Amyloid toxicity in Drosophila melanogaster*. May 2017. PhD thesis.

[7] Protein Data Bank. "1ZNI Insulin". `http://www.rcsb.org/3d-view/1ZNI/1`.

[8] F. Chiti et al. "Protein Misfolding, Functional Amyloid, and Human Disease". *Annual Review of Biochemistry*, 75(1):333–336, 2006.

[9] S. Treusch et al. "Amyloid deposits, Protection against toxic protein species?". *Cell Cycle*, 8(11):1668–1674, Jun 2009.

[10] J. Haradin et al. *Becker's World of the Cell*. Pearson, 8th edition, 2012.

[11] K. Arja et al. "Enhanced Fluorescent Assignment of Protein Aggregates by an OligothiophenePorphyrin-Based Amyloid Ligand". *macromolecular Journals*, 34.

[12] E. P. Azevedo et al. "Amyloid Fibrils Trigger the Release of Neutrophil Extracellular Traps (NETs), Causing Fibril Fragmentation by NET-associated Elastase". *The Journal of Biological Chemistry*, 287(44):37206–18, 26 Oct 2017.

[13] S. D. Styren et al. "X-34, A Fluorescent Derivative of Congo Red: A Novel Histochemical Stain for Alzheimer's Disease Pathology". *Journal of Histochemistry and Cytochemistry*, 48(9):1223–32, Sep 2000.

[14] K. M. Psonka-Antonczyk et al. "Nanoscopic and Photonic Ultrastructural Characterization of Two Distinct Insulin Amyloid States". *Int. J. Mol. Sci.*, 13.

[15] K. M. Psonka-Antonczyk et al. "Nanoscale Structure and Spectroscopic Probing of A1-40 Fibril Bundle Formation". *Frontiers in Chemistry*, 4(2):44, 2016.

[16] R. S. Dias et al. *Compendium in Molecular Biophysics*, 2017. Norwegian University of Science and Technology, Department of Physics.

[17] J. R. Albani. *Principles and Applications of Fluorescence Spectroscopy*. Blackwell Science, 1st edition, 2007.

[18] H. Lin et al. *Electronic Process in Organic Solids*. Visited 17.12.2017 `https://application.wiley-vch.de/books/sample/3527329684_c01.pdf`.

[19] J. McEwen (University of California Davis). *Jablonski diagram*. Visited 24.05.2018 `https://chem.libretexts.org/Core/Physical_and_Theoretical_Chemistry/Spectroscopy/Electronic_Spectroscopy/Jablonski$_$diagram`.

[20] J. R. Lakowicz. *Principles of Fluorescence Spectroscopy*. Kluwer Academic/Plenum Publishers, 2nd edition, 1999.

[21] H. Ecroyd et al. "Unraveling the Mysteries of Protein Folding and Misfolding,". *IUBMB Life*, 60(12):769–774, Des 2008.

[22] P. J. Thomas et al. "Defective protein folding as a basis of human disease". *Trends Biochem. Sci.*, 20(11):456–459, 1995.

[23] J. D. Sipe et al. "Amyloid fibril proteins and amyloidosis: chemical identification and clinical classification International Society of Amyloidosis 2016 Nomenclature Guidelines". *Amyloid*, 23(4):209–213, Nov 2016.

[24] R. Khurana et al. "Is Congo Red an Amyloid-specific Dye?". *Annual Review of Biochemistry*, 276(25):22715–22721, 2001.

[25] C. Caubet et al. "A new amyloidosis caused by fibrillar aggregates of mutated corneodesmosin". *The FASEB Journal*, 24(9):3416–3426, 2010.

[26] L. C. Serpell et al. "The protofilament substructure of amyloid fibrils". *Journal of Molecular Biology*, 300(5):1033–1039, Jul 2000.

[27] H. H. Bauer et al. "Architecture and Polymorphism of Fibrillar Supramolecular Assemblies Produced by in Vitro Aggregation of Human Calcitonin". *Journal of Structural Biology*, 115(1):1 – 15, Jul 1995.

[28] A. K. Buell et al. “Interactions between Amyloidophilic Dyes and Their Relevance to Studies of Amyloid Inhibitors”. *Biophysical Journal*, 99(10):3492–3497, Nov 2010.

[29] S. S. Mahshid et al. “A Highly Selective Electrochemical DNA-Based Sensor That Employs Steric Hindrance Effects to Detect Proteins Directly in Whole Blood”. *EJournal of the American Chemical Society,*, 137(50):15596–15599, 2015.

[30] M. I. Ivanova et al. “Molecular basis for insulin fibril assembly”. *PNAS*, 106(45):18990–18995, Nov 2009.

[31] Harvard.edu. *A Summary of Error Propagation*. Visited 17.12.2017 `http://ipl.physics.harvard.edu/wp-uploads/2013/03/PS3$_$Error$_$Propagation$_$sp13.pdf`.

[32] Dynamic Biosensors. *Binding Theory, Equations for Affinity and Kinetics Analysis*. Visited 23.04.2018 `http://www.dynamic-biosensors.com/wpcms/wp-content/uploads/2016/05/technote$_$101$_$binding-theory.pdf`.

[33] OLYMPUS. *Solvent Effects on Fluorescence Emission*. Visited 02.06.2018 `https://www.olympus-lifescience.com/en/microscope-resource/primer/java/jablonski/solventeffects/`.

[34] G. A. Reynolds et al. “New coumarin dyes with rigidized structure for flashlamp-pumped dye lasers”. *Optics Communications*, 13(3):222–225, 1975.

[35] A. M. Brouwer. “Standards for photoluminescence quantum yield measurements in solution”. *Pure and Applied Chemistry*, 83(12):2213–2228, 2011.

[36] et al. M. Y. Berezin. “Fluorescence Lifetime Measurements and Biological Imaging”. *Chem Rev*, 110(5):2641–2684, May 2010.

[37] X. L. Ho et al. “Fluorescence lifetime, dipole orientation and bilayer polymer films”. *Chemical Physics Letters*, 686.

[38] W. Becker. “Fluorescence lifetime imaging–techniques and applications”. *Journal of Microscopy*, 247(2):119–136, 2012.

[39] S. B. Raymond et al. “Smart optical probes for near-infrared fluorescence imaging of Alzheimers disease pathology”. *Eur. J. Nuc.l Med. Mol. Imaging*, 24(28):7210–7216, 2018.

[40] M. Albota et al. “Design of organic molecules with large two-photon absorption cross sections”. *Science*, 281(5382):1653–1656, 1998.

[41] M. Drobizhev et al. “Near-infrared two-photon absorption in phthalocyanines: Enhancement of lowest gerade-gerade transition by symmetrical electron-accepting substitution”. *The Journal of Chemical Physics*, 124(22):224701, 2006.

[42] J. Sjöqvist et al. “Molecular dynamics effects on luminescence properties of oligothiophene derivatives: A molecular mechanics-response theory study based on the CHARMM force field and density functional theory”. *Phys. Chem. Chem. Phys.*, 13.

Appendix

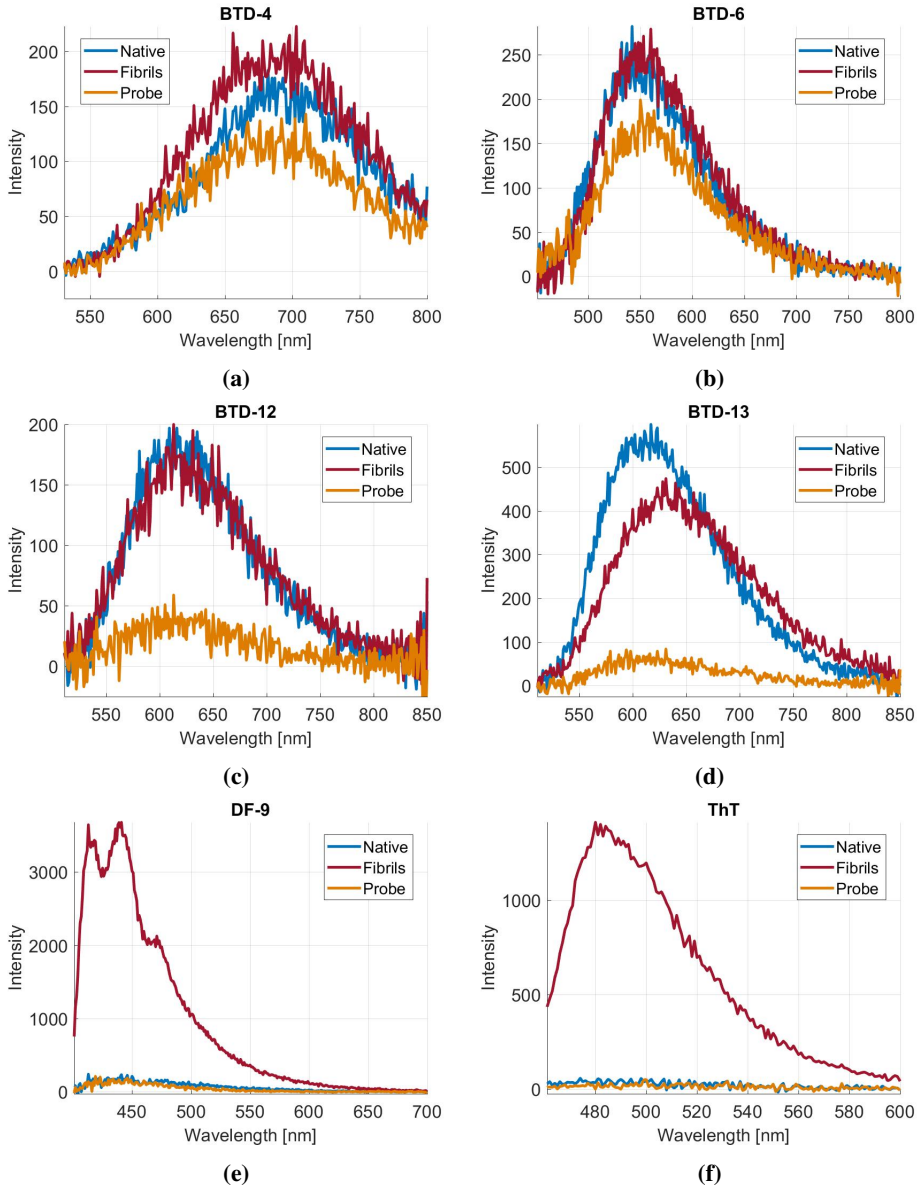

Figure 6.1: Emission spectra upon binding to fibrillar and native insulin.

Six new dyes were syntehized and measured towards the end of the semester.

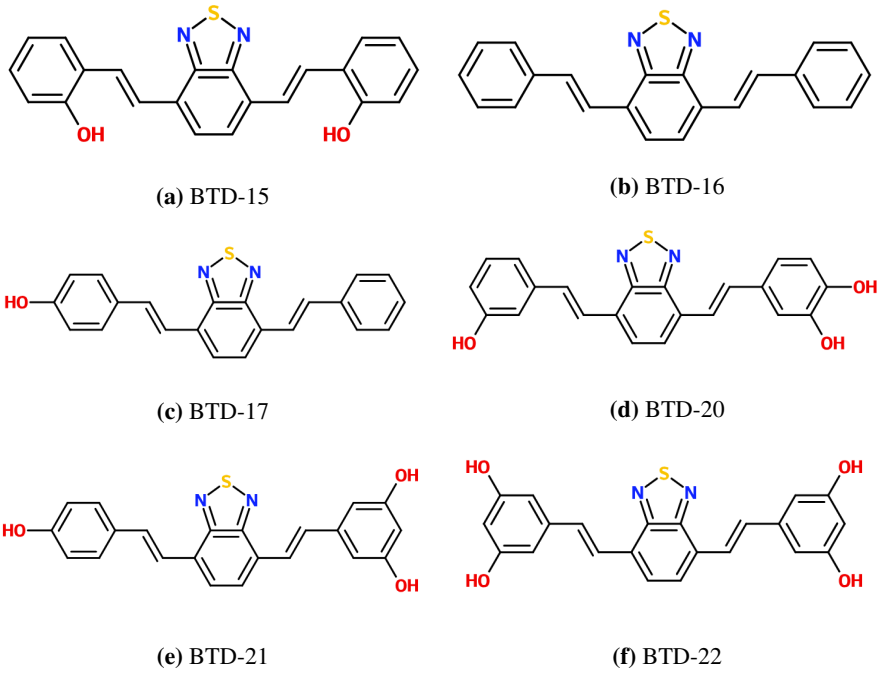

(a) BTD-15 **(b)** BTD-16

(c) BTD-17 **(d)** BTD-20

(e) BTD-21 **(f)** BTD-22

Figure 6.2: The structures of the probes. Drawn using the program eMolecules [4].

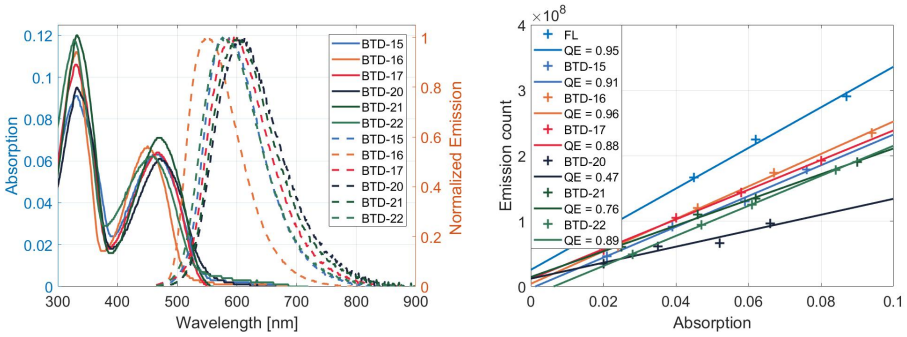

(a) **(b)**

Figure 6.3: The absorption and emission spectra are show in a. The linear relation between absorption and emission is shown in b.

Sample	ε_{max1}	λ_{abs1}	ε_{max2}	λ_{abs2}	λ_{em}	Stokes shift	Quantum yield
	$[(Mcm)^{-1}]$	$[nm]$	$[(Mcm)^{-1}]$	$[nm]$	$[nm]$	$[nm]$	-
BTD-15	27 300	330	18 900	460	580	120	0.91 ± 0.05
BTD-16	33 600	331	20 100	451	550	99	0.96 ± 0.05
BTD-17	31 800	330	19 200	466	595	129	0.88 ± 0.04
BTD-20	28 500	332	18 300	470	613	143	0.47 ± 0.07
BTD-21	36 000	332	21 300	467	601	134	0.76 ± 0.04
BTD-22	35 100	328	18 600	454	576	122	0.89 ± 0.04

Table 6.1: Summary of the photo-physical properties of the new dyes in toluene.

Sample	B_1	t_1	B_2	t_2	τ_{gave}	τ_{ave}
	$\%$	ns	$\%$	ns	ns	ns
BTD-15	47	4.1 ± 0.6	53	7.2 ± 0.3	6.2	5.7
BTD-16	46	7.0 ± 0.3	54	4.6 ± 0.3	6.0	5.7
BTD-17	45	7.8 ± 0.3	55	4.9 ± 0.3	6.5	6.2
BTD-20	9	3.1 ± 0.1	91	6.1 ± 0.2	6.0	5.8
BTD-21	30	4.0 ± 0.9	70	7.2 ± 0.2	6.6	6.2
BTD-22	30	4.1 ± 0.8	70	7.5 ± 0.2	6.9	6.5

Table 6.2: Lifetimes in Toluene. τ_{gave} is the geometric average.